RESEARCH

Optimization of transverse electro-optic effect in LiNbO$_3$ and LiTaO$_3$ crystals

Ji-Fang Shang[1,2] · Qing-Lian Li[3] · Fu-Xiao Zhang[1,2] · Ning-Zhe Niu[1,2] · Ling Chen[1,2] · Wen-Jing Du[1,2]

Abstract

We analyze the transverse electro-optic (EO) effect in an arbitrary direction in LiNbO$_3$ (LN) and LiTaO$_3$ (LT) crystals based on the Fresnel index ellipsoid theory. A set of analytical formulas for calculating the birefringence in any direction in a crystal of the lowest symmetry is first deduced. The maximum magnitudes of the transverse EO effect appear along the directions that are turned out from the optic axis on the angles θ_m ($\varphi = 30°$, 150° or 270°) or $180° - \theta_m$ ($\varphi = 90°$, 210° or 330°), the angles θ_m of congruent LN and LT crystals are 36° and 59.5°, respectively. For experimental verification, the (yzw)θ_m cut congruent LN and LT crystals were prepared. The half-wave voltage (HWV) of the (yzw)36° cut LN crystals is half that of the x-cut LN crystals and is only 30% that of the z-cut LN crystals, and the HWV of the (yzw)59.5° cut LT crystals is 7% higher than that of the x-cut LT crystals, the experimental results agree well with the theoretical analysis. The crystals with the optimized cell geometries are more practical because of the low HWV and lower sensitivity of birefringence to temperature.

1 Introduction

Lithium niobate (LiNbO$_3$, LN) crystals are one of the few practical electro-optic (EO) crystals, which have the advantages of easy to grow, large EO coefficients, non-deliquescence, easy processing, etc. [1–4]. In the past few decades, LN crystals have been extensively used for EO devices including EO modulators, EO Q-switches, EO slitters, etc.

✉ Qing-Lian Li
  liqlnankai@163.com

  Ji-Fang Shang
  shangjf@haue.edu.cn

  Fu-Xiao Zhang
  3424912615@qq.com

  Ning-Zhe Niu
  nkshang@qq.com

  Ling Chen
  cling555@163.com

  Wen-Jing Du
  duer0911@sina.com

1 Henan Key Laboratory of Electronic Ceramic Materials and Application, Henan University of Engineering, Zhengzhou 451191, China

2 College of Materials Engineering, Henan University of Engineering, Zhengzhou 451191, China

3 School of Physics, Nankai University, Tianjin 300071, China

[5–7]. The conventional LN EO devices are usually made of their so-called direct cuts with the directions of the applied electric field and light propagation along the principal crystallographic axes [8, 9]. In such geometries, the maximum effective EO coefficient is not utilized or a considerable phase difference induced by natural birefringence is introduced which is sensitive to temperature [10]. Lithium tantalate (LiTaO$_3$, LT) crystals are isomorphic to LN and also possess excellent EO properties, even better, the laser damage threshold of LT crystals is about five times larger than that of LN crystals [11]. Unfortunately, the EO coefficient γ_{22} is only 0.1 pm/V [12], which results in the unavailability of the transverse EO modulation with light propagating along the optic axis. Therefore, there is little research on the EO application of LT crystals [13, 14].

Currently, little attention has been paid to the spatial anisotropy of the transverse EO effect in LN and LT crystals, which limits the development and application of EO devices with low half-wave voltage (HWV) and high performances. Su et al. studied the EO effect in an arbitrary propagation direction in LN crystal, but the voltage was only applied to the x or y direction [15]. The direction of the applied electric field is not perpendicular to the light propagation direction, which is adverse to optical processing and application. Zhang et al. proposed a set of analytical phase shift formulas in electro-optical crystals with an arbitrary incident direction, but the electric field was also only applied along the x-axis [16]. Yan

et al. derived the transverse dielectric tensor matrix in any direction in LN crystals utilizing the second-order nonlinear polarization but only analyzed the rotation of eigenpolarization directions when the light propagation and applied voltage are along the principal dielectric axes [17]. Song et al. only calculated the birefringence for the light propagating near the optic axis and the voltage is applied perpendicular to the optic axis in LN crystals [18]. A. S. Andrushchak and co-workers proposed indicative surfaces describing the spatial anisotropy of the longitudinal and transverse linear EO effects in LN crystals, however, the direction of the applied electric field is limited within or perpendicular to the principal plane [19].

In this work, we conduct an accurate analysis of the birefringence in any direction in a crystal of the lowest symmetry and derive the general formulas for calculating birefringence. On this basis, we analyze the transverse EO effect in an arbitrary direction in LN and LT crystals. The optimized geometries suitable for EO applications are determined. LN and LT crystals with the optimized geometries were prepared and their HWV was measured.

2 Methods

2.1 Birefringence in an arbitrary direction in a crystal of the lowest symmetry

Based on the Fresnel index ellipsoid theory [20], the index ellipsoid equation in a crystal of the lowest symmetry can be expressed as

$$\beta_{11}x^2 + \beta_{22}y^2 + \beta_{33}z^2 + 2\beta_{23}yz + 2\beta_{13}xz + 2\beta_{12}xy = 1 \quad (1)$$

where x, y, and z axes along each principal crystallographic axis respectively, β_{ij} (i, j = 1, 2 or 3) are the optical impermeability tensor components. For an arbitrary propagation direction that can be described by the polar angle θ and the azimuth angle φ, the birefringence and corresponding eigenpolarization directions can be determined by the principal axes of the ellipse section that is perpendicular to the propagation direction. As shown in Fig. 1, we define a rotated coordinate system $x'y'z'$, the z'-axis is chosen to be parallel to the wave normal k, and the x'-axis lies in the plane containing z and z'. Using the coordinate transformation and taking the terms containing z' as zero, one can obtain the elliptic equation.

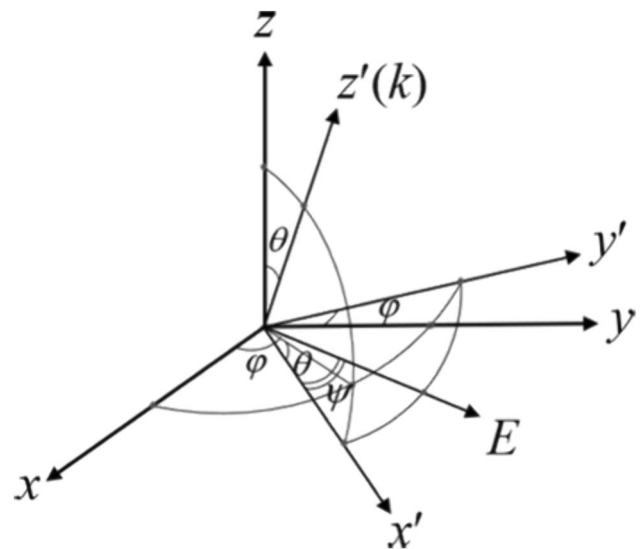$$Ax'^2 + By'^2 + Cx'y' = 1 \quad (2)$$

Fig. 1 Spatial position of the rotating coordinate system x', y', z' with respect to the crystallophysical coordinate system x, y, z. k represents wave normal direction, and E represents the direction of an applied electric field

$$
\begin{aligned}
A = {} & \beta_{11}\cos^2\theta\cos^2\varphi + \beta_{22}\cos^2\theta\sin^2\varphi + \beta_{33}\sin^2\theta \\
& - 2\beta_{23}\sin\theta\cos\theta\sin\varphi - 2\beta_{13}\sin\theta\cos\theta\cos\varphi \\
& + 2\beta_{12}\cos^2\theta\sin\varphi\cos\varphi \\
B = {} & \beta_{11}\sin^2\varphi + \beta_{22}\cos^2\varphi - 2\beta_{12}\sin\varphi\cos\varphi \quad (3) \\
C = {} & -2\beta_{11}\cos\theta\cos\varphi\sin\varphi + 2\beta_{22}\cos\theta\sin\varphi\cos\varphi \\
& - 2\beta_{23}\sin\theta\cos\varphi + 2\beta_{13}\sin\theta\sin\varphi \\
& + 2\beta_{12}\cos\theta\cos^2\varphi - 2\beta_{12}\sin^2\varphi\cos\theta
\end{aligned}
$$

Let the principal axes of the ellipse at an angle α to the $x'(y')$ axis, the angle α can be calculated as

$$\tan 2\alpha = \frac{C}{A - B} \quad (4)$$

The principal axes are the directions of the two permitted vibrations, namely, eigenpolarization directions. The birefringence n_1 and n_2 are determined to be

$$
\frac{1}{n_1^2} = \frac{A + B}{2} + \frac{\sqrt{(A - B)^2 + C^2}}{2}
$$

$$
\frac{1}{n_2^2} = \frac{A + B}{2} - \frac{\sqrt{(A - B)^2 + C^2}}{2}
$$

$$(5)$$

2.2 Transverse EO effect in an arbitrary propagation direction in LN and LT crystals

In transverse configuration, the direction of the applied electric field is perpendicular to the light propagation direction, therefore the applied electric field lies in the x'–y' plane. Let the direction of the electric field E is at an angle of ψ to the x'-axis, the electric field components in the principal crystallophysical system can be expressed as

$$E_x = E \cos\psi \cos\theta \cos\varphi - E \sin\psi \sin\varphi$$
$$E_y = E \cos\psi \cos\theta \sin\varphi + E \sin\psi \cos\varphi \qquad (6)$$
$$E_z = -E \cos\psi \sin\theta$$

Based on the EO effect of LN and LT crystals [21], the optical impermeability tensor can be determined. Combining with Eqs. (3)–(6), one can obtain the induced birefringence and the corresponding eigenpolarization directions in any direction. The magnitude of field-induced birefringence is the difference between the values when an electric field is applied and not applied.

2.3 Preparation of the (*yzw*)*θ*ₘ cut congruent LN and LT crystals and measurement of HWV

Based on the theoretical results of spatial anisotropy of the transverse EO effect, the optimized geometries of EO cell are determined to be $(yzw)\theta_m$, $(xzlw)-30°/-\theta_m$ or $(xzlw)30°/\theta_m$ cut, the angles θ_m of congruent LN and LT crystals are 36° and 59.5°, respectively. The notation of cut type is defined in the IEEE standard [22]. LN and LT crystals were $(yzw)\theta_m$ cut with dimensions of 8.3 mm × 8.3 mm × 4 mm and 7.8 mm × 7.8 mm × 10 mm ($t \times w \times l$), respectively. Figure 2 illustrates the $(yzw)\theta_m$ cut crystals. The crystal faces were oriented with an angle precision of ± 5 arc minutes. For the $(yzw)36°$ cut LN crystals, the faces that are perpendicular to the directions of light propagation and applied electric field were oriented with the aid of the $\left(0\bar{1}4\right)$ and (012) crystallographic planes respectively, and the faces of the $(yzw)59.5°$ cut LT crystals were oriented with the aid of the $\left(0\bar{3}6\right)$ and (018) crystallographic planes respectively. The orientation method was explained in the literature [23]. Each face of the crystals was finely ground, and the transmission surfaces were precisely polished. The two end faces in the thickness direction were plated with silver. The same crystals were used in a compensating mode to eliminate natural birefringence, their thickness or width directions (t or w) are perpendicular to each other. The applied voltage is equal in magnitude but opposite in direction.

The HWV was measured by using extremum method [24], the configuration is shown in Fig. 3. A Nd:YAG
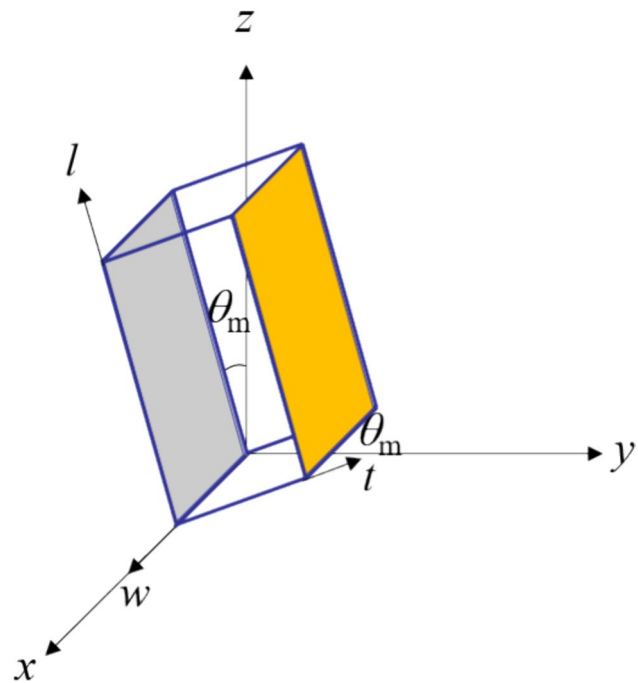

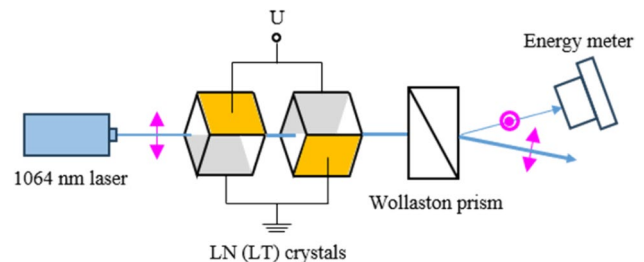**Fig. 2** Illustration of the $(yzw)\theta_m$ cut crystals

Fig. 3 Experimental setup for measuring the half-wave voltage of $(yzw)\theta_m$ cut LN and LT double crystals

pulsed laser with a wavelength of 1064 nm, a pulse width of 10 ns and a repetition rate of 1 Hz was used. The beam diameter is 5 mm with a divergence angle of less than 5 mrad, the energy jitter is less than 3%. The laser is polarized along the horizontal direction. The laser is normally incident upon the surface of the crystals, and the laser polarization direction is at an angle of 45° to the thickness or width direction of the crystals. A Wollaston prism was used as an analyzer, the transmission direction of the analyzer was kept perpendicular to the polarization direction of the laser. The transmitted energy was measured by a laser energy meter. An adjustable high DC voltage was applied to the double crystals.

3 Results and discussion

3.1 Spatial anisotropy of the transverse EO effect in LN and LT crystals

Based on the theoretical analysis, the transverse EO effect in any propagation direction in LN and LT crystals was simulated and computed. The magnitude of electric field E was taken as 10^6 V/m, the refractive indices and EO coefficients of congruent LN and LT crystals were taken from the literature [11, 25, 26], and the constant strain (clamped) EO coefficients γ^S were used. For each propagation direction, the field-induced birefringence is found to vary with the direction of applied voltage in a sine form, as shown in Fig. 4. The maximum induced birefringence (MIB) and the corresponding direction of applied voltage (optimal voltage direction, OVD) vary with the propagation directions. Furthermore, except for in some certain directions, the angle ψ between the OVD and the x'-axis is verified to be not 0°, 180° or 90°, namely, the OVDs are not along the x'- or y'-axis, which is different from that in the literature [19].

The OVD for each direction was calculated, the result is shown in Fig. 5a. The OVD varies periodically with the angle φ with a period of $2\pi/3$. In the directions at a small angle to the optic axis ($\theta \leq 45°$ or $\theta \geq 135°$), the OVDs are closely related to both the angles φ and θ. The difference in OVDs for different angles φ gradually decreases as the propagation direction gradually deviates from the optic axis. In the directions that deviate significantly from the optic axis ($45° \leq \theta \leq 135°$), the OVDs appear to be independent of the
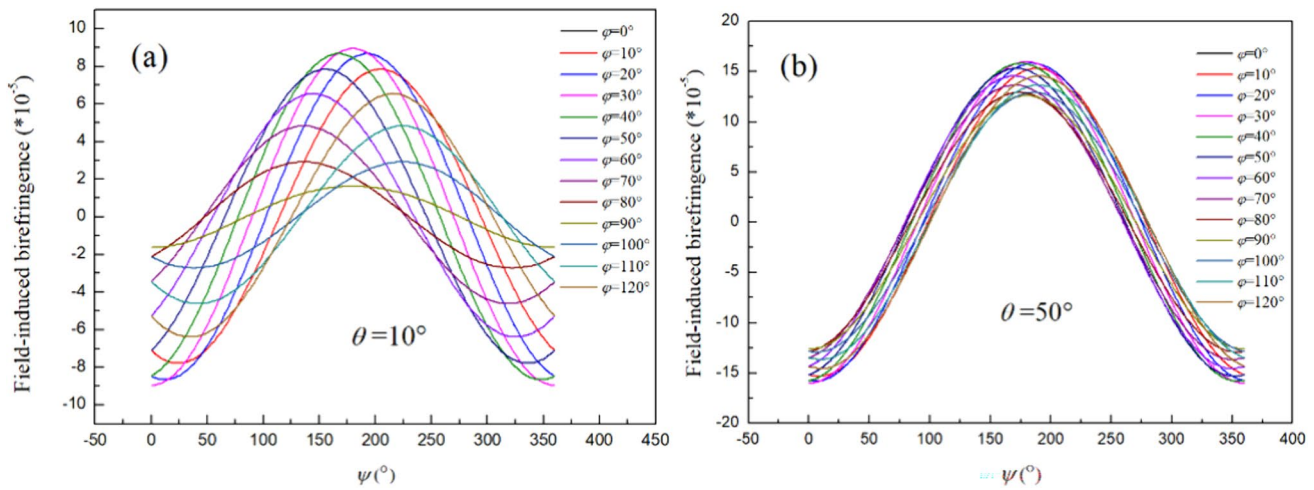
Fig. 4 The variation of induced birefringence with the direction of applied voltage for multiple angles φ in LN crystal. **a** $\theta = 10°$; **b** $\theta = 50°$

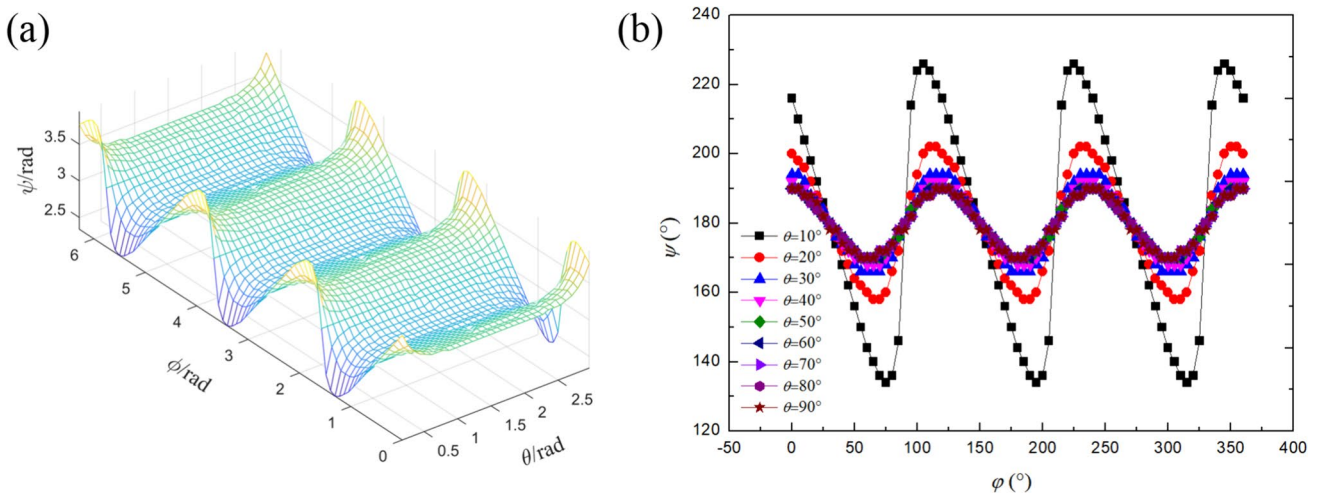**Fig. 5** Spatial variation of the OVDs. **a** Three-dimensional distribution; **b** variation with the angles φ for multiple angles θ

angle θ, and the difference in OVDs for different angles φ is minimized. The variation in OVDs with the angles φ for multiple angles θ is shown in Fig. 5b. The maximum angle between the OVD and the x'-axis is up to 46° for an angle θ of 10°, while the maximum angle is only 10° when the propagation direction is away from the optic axis.

Figure 6 presents the MIB for each propagation direction in LN crystals in the spherical coordinate system, where the length of the radius vector represents the magnitude of MIB. The indicative surface describing the MIB in any direction is characterized by the point group symmetry 3 m, which follows the symmetry of the crystal structure of LN. In the directions at a small angle to the optic axis, the MIB varies significantly with angles φ, and the extreme values occur at $\varphi = 30° + n\,60°$ ($n = 0, 1, 2, \ldots$). The difference in MIB for different angles φ gradually decreases as the propagation direction gradually deviates from the optic axis.

The maximal magnitude of the MIB appears in the directions that are turned out from the optic axis on the angles $\theta_m = 139.5°$ ($\varphi = 90°$, 210° or 330°) or $\theta_m = 40.5°$ ($\varphi = 30°$, 150° or 270°), and the corresponding OVDs appear along the x'-axis. With the same magnitude of applied voltage, the MIB at these directions (1.654×10^{-4}) exceeds about 53.7% the magnitude of the induced birefringence along the x'-axis (1.076×10^{-4}), and more than four times the one along the optic axis (3.78×10^{-5}). This results in a corresponding reduction of the driving voltage of EO devices. Furthermore, the rotation angle α of the permitted vibrations of the induced birefringence relative to the principal plane is calculated to be zero, namely, the two eigenpolarization directions are along the x'- and y'-axes, respectively. In addition, the MIB at low frequencies was also calculated, the maximum value appears in the directions

that are turned out from the optic axis on the angles $\theta_m = 144°$ ($\varphi = 90°$, 210° or 330°) or $\theta_m = 36°$ ($\varphi = 30°$, 150° or 270°), the constant stress (unclamped) EO coefficients γ^T were taken from the literature [27]. The results are consistent with the simulation results in the literature [19]. With the same magnitude of applied voltage, the MIB at these directions (2.064×10^{-4}) is almost twice the one along the x-axis (1.015×10^{-4}), and almost three times exceeds the one along the optic axis (7.56×10^{-5}).

Similarly, we have determined the spatial anisotropy of the transverse EO effect in LT crystals. Since the similar crystal structure of LT and LN crystals, the MIB and the corresponding OVD exhibit a similar dependence on the propagation directions, as shown in Fig. 7. The magnitudes of MIB and OVD in each propagation direction are different in the two crystals. The maximum angle ψ of the OVD is 29° for an angle θ of 10°, while the maximum angle ψ is only about 3° when the propagation direction is away from the optic axis. The maximal magnitude of the MIB appears along the directions that are turned out from the optic axis on the angles $\theta_m = 59.5°$ ($\varphi = 30°$, 150° or 270°) or $\theta_m = 120.5°$ ($\varphi = 90°$, 210° or 330°), and the corresponding OVDs are also along the x'-axis. With the same magnitude of applied voltage, the MIB at these directions (1.193×10^{-4}) is a little larger than that along the x-axis (1.14×10^{-4}). Besides, the two eigenpolarization directions are also along the x'- and y'-axes, respectively. The MIB at low frequencies was not calculated because the magnitude of the EO coefficient γ_{51}^T was not determined in previous literature [28, 29].

In addition, we also analyze the temperature sensitivity of natural birefringence in different directions of light propagation. In a uniaxial crystal, the natural birefringence in the direction with a polar angle θ can be expressed as [20]
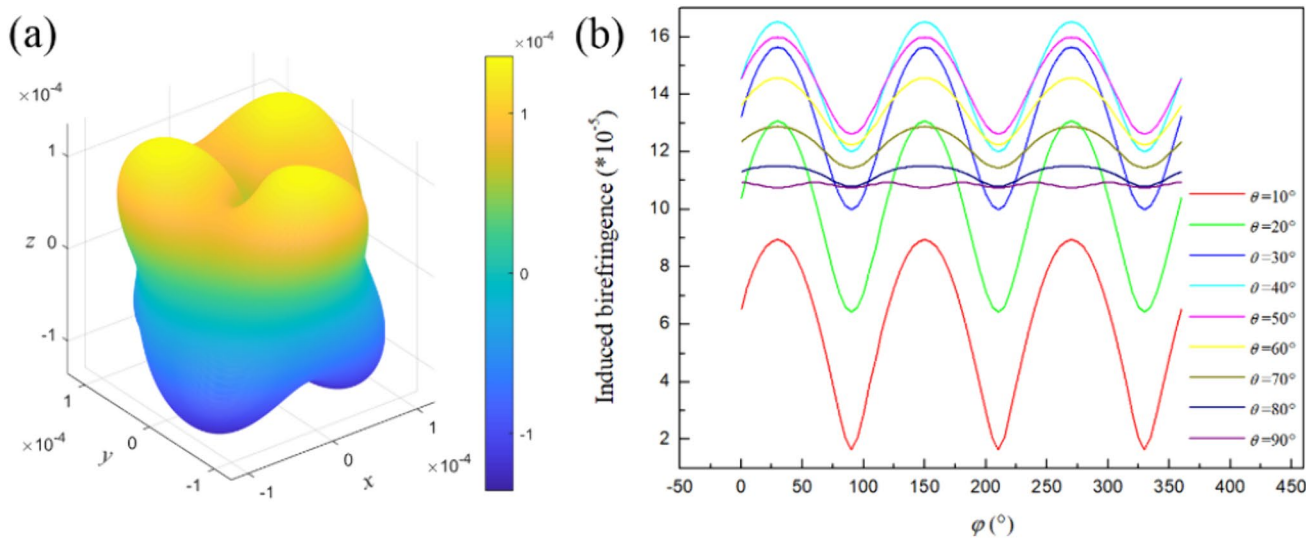

Fig. 6 Spatial variation of the MIB. **a** Three-dimensional distribution; **b** variation with the angles φ for multiple angles θ
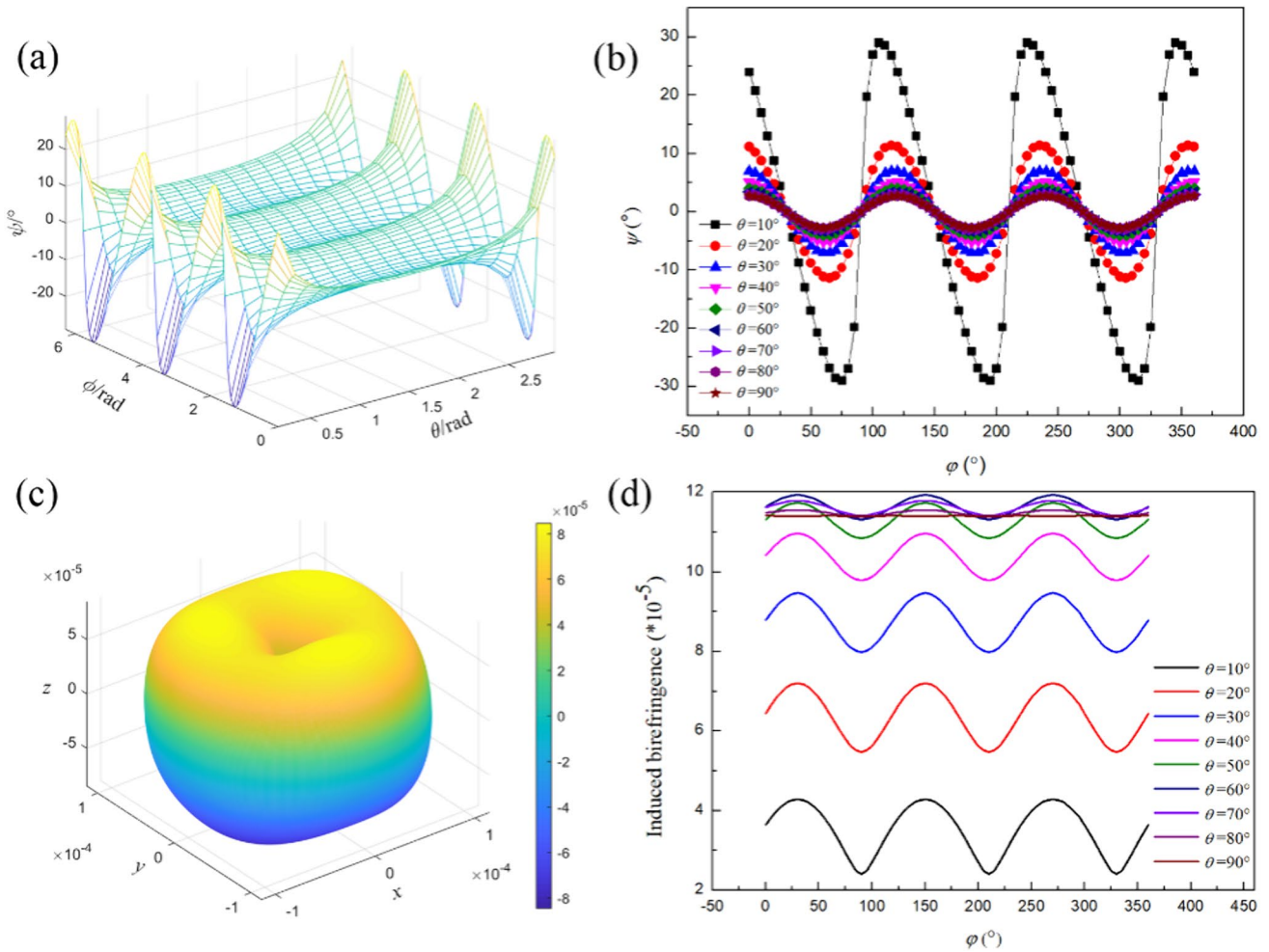
Fig. 7 Spatial variation of the OVD and MIB in LT crystals. **a** Three-dimensional distribution of the OVDs; **b** variation in OVD with angles φ for multiple angles θ; **c** three-dimensional distribution of the MIB; **d** variation in MIB with angles φ for multiple angles θ

$$\Delta n = n_o - \left(\frac{\cos^2 \theta}{n_o^2} + \frac{\sin^2 \theta}{n_e^2} \right)^{-\frac{1}{2}} \approx \frac{\Delta n_o^3 \sin^2 \theta}{2} \quad (7)$$

where n_o and n_e are the ordinary and extraordinary refractive indices, $\Delta = 1/n_e^2 - 1/n_o^2$. The temperature sensitivity of natural birefringence can be calculated as

$$\frac{\partial \Delta n}{\partial T} = \left(1 - \frac{n_{e'}^3(\theta)}{n_o^3} \cos^2 \theta \right) \frac{\partial n_o}{\partial T} - \frac{n_{e'}^3(\theta)}{n_e^3} \sin^2 \theta \frac{\partial n_e}{\partial T}$$

$$\approx \sin^2 \theta \frac{\partial (n_o - n_e)}{\partial T} \quad (8)$$

where $n_{e'}(\theta)$ represents the extraordinary refractive index in the direction with a polar angle θ. The magnitude of natural birefringence and its temperature sensitivity are both directly proportional to $\sin^2\theta$. For EO applications, it is necessary to use a second crystal rotated by 90° concerning the first crystal to compensate for the natural birefringence

and to eliminate its thermal fluctuations. As determined in our previous work [30], the tolerance of length deviation between the two matching crystals is inversely proportional to the magnitude of natural birefringence, and the tolerance of temperature difference is inversely proportional to the temperature sensitivity of natural birefringence. Therefore, the cell geometry with the direction of light propagation close to the optic axis is more practical because of the large tolerances.

3.2 HWV of congruent LN and LT double crystals

In the orthogonal polarization configuration, the transmitted energy varies with the applied voltage in a sine-squared form, as shown in Fig. 8. The HWV of the LN and LT double crystals is measured to be 2900 V and 2300 V, respectively. With the same dimensions, the HWV of the $(yzw)36°$ cut LN crystal is nearly half that of the x-cut LN crystal and is only about 30% that of the commercial z-cut LN crystal,
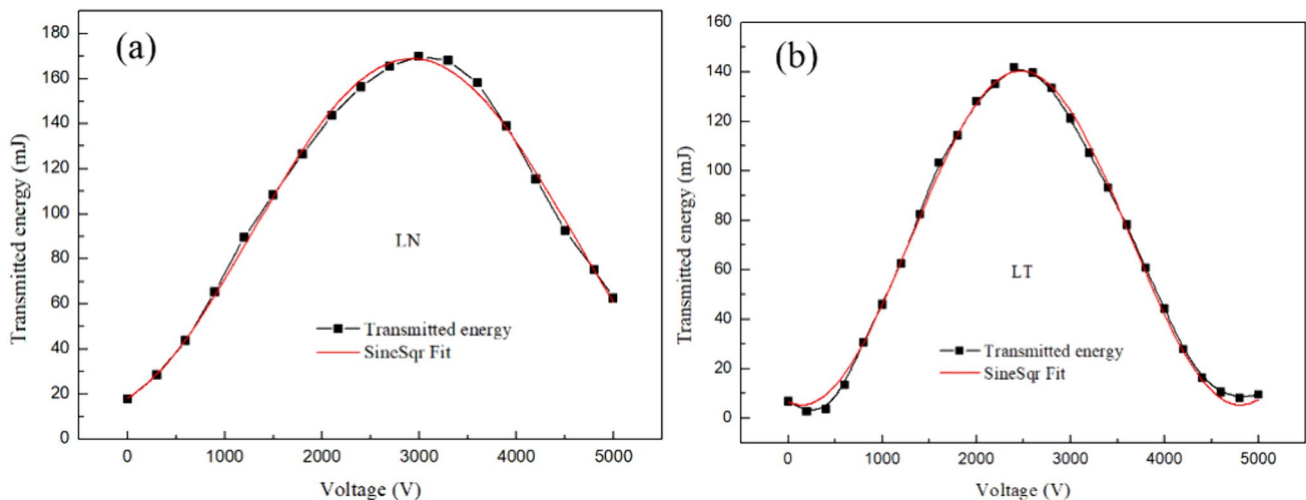
Fig. 8 Variation in transmitted energy with applied voltage. **a** LN double crystals; **b** LT double crystals

which is in good agreement with the theoretical analysis. The HWV of the (yzw)59.5° cut LT crystal is 7% larger than the one (2150 V) of the x-cut LT crystal. Based on the experimental result, the unclamped EO coefficient γ_{51}^T of LT is estimated to be 15.1 pm/V, which is close to the value (15 pm/V) measured at a wavelength of 3.3913 μm [27]. Despite the slightly higher driving voltage, the (yzw)59.5° cut LT crystals are more practical because of the less sensitivity of birefringence to temperature.

In addition, we also analyzed the influence of cutting accuracy on the performance properties of EO cells. In the manufacture of optical elements, the practical crystallographic orientation may deviate from the desired orientation, which may result in a change in the magnitude of induced birefringence and the eigenpolarization directions. For a cutting accuracy of one degree, the maximum variation in induced birefringence of the (yzw)36° cut LN crystals was calculated to be 3.8×10^{-6}, which is only 1.8 percent of the MIB, and the rotation angle α of the eigenpolarization directions to the principal plane is only 0.44 arc minutes. For the (yzw)59.5° cut LT crystals, the maximum variation in induced birefringence (1.38×10^{-6}) is only 1.2 percent of the MIB, and the rotation angle α of the eigenpolarization directions is 2.2 arc minutes. In our work, the faces of the (yzw)θ_m cut crystals were oriented with an angle precision of ± 5 arc minutes. Therefore, the influence of cutting accuracy is negligible.

It should be noted that the above theoretical analysis and experimental results are mainly focused on the performance properties of the congruent crystals at a wavelength of 1064 nm. Owning to the dependencies of refractive indices and EO coefficients on composition, wavelength, temperature, frequency, etc., the optimized cell geometries and the maximal magnitude of the MIB may be different

in different cases. Using the methodology developed in the present work, the optimized geometry can be in principle found for any other cases, including for other crystal materials with arbitrary symmetry.

4 Conclusions

We have presented the results of spatial anisotropy of the transverse EO effect in LN and LT crystals and derived the optimized cell geometries suitable for EO applications. The field-induced birefringence for each propagation direction was found to vary with the direction of applied voltage in a sine form. The MIB and OVD in the two crystals show a similar dependence on the propagation directions. The maximum magnitudes of the transverse EO effect appear along the directions that substantially deviate from the principal crystallographic axes. Compared to the conventional x-cut or z-cut LN crystals, the HWV of the LN crystals with the optimized cell geometries is decreased by $2 \sim 4$ times. Despite the slightly higher HWV of the (yzw)59.5° cut LT crystal than the x-cut LT crystal, it is more practical because of the lower sensitivity of birefringence to temperature. These results are of great significance for the development of LN and LT EO devices with high performances. Furthermore, the derived analytical formulas for calculating the birefringence in any direction in a crystal of the lowest symmetry are suitable for all the birefringent crystals.

Declarations

References

1. M. Yu, R. Cheng, C. Reimer, L. He, K. Luke, E. Puma, L. Shao, A. Ansari, X. Ren, H. Grant, L. Johansson, M. Zhang, M. Loncar, Nat. Photon. **17**, 666 (2023)
2. A. Paliwal, A. Sharma, R. Guo, A.S. Bhalla, V. Gupta, M. Tomar, Appl. Phys. B **125**, 115 (2019)
3. J.F. Shang, J. Sun, Q.L. Li, J.F. Yang, L. Zhang, J.J. Xu, Sci. Rep. **7**, 4651 (2017)
4. J. Sun, Y.X. Hao, L. Zhang, J.J. Xu, S.N. Zhu, J. Synth. Cryst. **49**, 947 (2020)
5. J.F. Shang, J.F. Yang, H.S. Hao, Q.L. Li, L. Zhang, J. Sun, Opt. Express **28**, 22287 (2020)
6. J.H. Li, K.X. Chen, Appl. Phys. B **129**, 39 (2023)
7. J. Wu, Q.L. Li, Z.Z. Zhang, J. Sun, L. Zhang, Z. Sui, J.J. Xu, Chin. J. Lasers **49**, 0708001 (2022)
8. H. Feng, K. Zhang, W. Sun, Y. Ren, C. Wang, Photonics Res. **10**, 2366 (2022)
9. M. Mandal, S. Mukhopadhyay, Optoelectron. Lett. **16**, 338 (2020)
10. J.P. Salvestrini, M. Abarkan, M.D. Fontana, Opt. Mater. **26**, 449 (2004)
11. M. Roth, M. Tseitlin, N. Angert, Glass Phys. Chem. **13**, 86 (2005)
12. M. Abarkan, J.P. Salvestrini, M.D. Fontana, M. Aillerie, Appl. Phys. B **76**, 765 (2003)
13. Q.L. Li, J.F. Shang, J. Wu, L. Zhang, J. Sun, J. Synth. Cryst. **48**, 812 (2019)
14. B.L. Davydov, A.A. Krylov, D.I. Yagodkin, Quantum Electron. **37**, 484 (2007)
15. S. Su, L. Wan, Y. Zhou, J. Sun, L. Liu, Acta Optica Sinica **30**, 2972 (2010)
16. P. Zhang, X. Du, Y. Song, J. Wu, J. Sun, J. Phys. D Appl. Phys. **53**, 095306 (2020)
17. Y. Yan, C. Wu, L. Liu, J. Wang, Z. Huang, Optics Optoelectron. Technol. **16**, 33 (2018)
18. Z. Song, L. Liu, Y. Zhou, D. Liu, H. Ren, Chin. J. Lasers **32**, 319 (2005)
19. A.S. Andrushchak, B.G. Mytsyk, N.M. Demyanyshyn, M.V. Kaidan, O.V. Yurkevych, S.S. Dumych, A.V. Kityk, W. Schranz, Opt. Laser Eng. **47**, 24 (2009)
20. Q.T. Liang, *Physical Optics* (Electronics Industry Press, Beijing, 2018)
21. D.N. Nikogosyan, *Nonlinear Optical Crystals: A Complete Survey* (Springer, Berlin, Heidelberg, 2005)
22. IEEE, "ANSI/IEEE Std. 176–1987: IEEE Standard on Piezoelectricity," The Institute of Electrical and Electronics Engineers, 25 (1988)
23. C.L. Guo, J. Chin. Ceram. Soc. **9**, 408 (1981)
24. J. Sun, H. Mou, S. Liu, Y. Li, Y. Zhang, Optoelectron. Technol. **27**, 212 (2007)
25. E.H. Turner, Appl. Phys. Lett. **8**, 303 (1966)
26. G. Wang, B. Hu, Y. Chen, H. Xia, Y. Zhu, J. Synth. Cryst. **20**, 189 (1991)
27. A. Yariv, P. Yeh, *Optical Waves in Crystals* (John Wiley & Sons, Hoboken, 1984)
28. K. Onuki, N. Uchida, T. Saku, J. Opt. Soc. Am. **62**, 1030 (1972)
29. P.V. Lenzo, E.H. Turner, E.G. Spencer, A.A. Ballman, Appl. Phys. Lett. **8**, 81 (1966)
30. J.F. Shang, Q.L. Li, X. Sun, L. Chen, W.J. Du, L.B. Li, Chin. J. Lasers **51**, 0801002 (2024)